Biomaterials Science

ROYAL SOCIETY OF CHEMISTRY

PAPER

View Article Online
View Journal

Cite this: DOI: 10.1039/d5bm01812a

Engineering immunostimulatory nanocarriers: TLR7-agonist conjugated poly(beta-amino ester) mRNA delivery systems

Hulya Bayraktutan, [a,b,c] Amr ElSherbeny, [a,b] Rafał J. Kopiasz, [a,d] Charlotte Galley,[e] Nurcan Gumus, [a,b,f,g] Clare L. Bennett,[e] Cameron Alexander *[a] and Pratik Gurnani *[h]

Messenger RNA (mRNA) technology serves as a powerful foundation for novel vaccines and treatments. Ensuring the effective delivery of RNA medicines requires vectors due to the poor cellular association of naked mRNA and its susceptibility to degradation by endogenous nucleases. Recently, nanoparticle-based carriers have attracted significant attention, particularly poly(beta-amino esters) (PBAEs), which have shown promise as mRNA delivery systems. The first generation of nanoparticle-encapsulated mRNA vaccines has been highly successful in protecting against severe COVID-19 disease, but the durability of the immune response remains short; hence, there is a need for delivery systems that enhance the robustness of the immune response. In this study, we report the development of a TLR7-adjuvanting PBAE through the direct conjugation of Loxoribine, a potent TLR7 agonist. We observed that the Loxoribine-conjugated PBAE was able to condense self-amplifying RNA (saRNA) efficiently into small (100–200 nm) polyelectrolyte nanoparticles with complete incorporation of the nucleic acid. Formulations specifically at a w/w ratio of 128 showed high transfection in HEK293T and DC2.4 cell lines with good cytotoxicity profiles. In addition, TLR activation assays using TLR7 reporter HEK-Blue cells showed that Loxoribine-conjugated formulations can efficiently agonise TLR7, with some synergy observed between Loxoribine and the delivered saRNA. Although potent activation was observed in model cell lines, evaluation in primary bone marrow-derived dendritic cells showed minimal upregulation of CD86, an established activation marker, and a transfection efficiency of less than 2%. Consequently, these findings suggest the potential of adjuvanted PBAE nanoparticles for enhanced RNA vaccines; however, further development is needed to improve their activity in primary immune cells.

Received 11th December 2025,
Accepted 11th April 2026

DOI: 10.1039/d5bm01812a

rsc.li/biomaterials-science

Introduction

Messenger RNA technology represents a safe, potent and manufacturer-friendly route to express transiently endogenous or engineered proteins in target cells or tissues. Therefore, mRNA has been widely studied for the development of novel vaccines against infectious diseases and immunotherapies for a variety of malignancies.[1,2] These vaccines operate by administering mRNA encoding pathogen or malignant cell surface protein epitopes to train the immune system to recognise and eliminate cells expressing them, either upon infection by the pathogen or in cancer tumours/cells.[3,4] In both applications, the quality and robustness of the immune response are critical to the eventual adaptive immune response against the target antigen and therefore to the therapeutic/prophylactic performance.

Naked mRNA displays poor cellular association and is susceptible to degradation by endogenous nucleases, indicating that a suitable delivery vector is required to protect the nucleic acid cargo and facilitate its transportation to its target in the

[a]Division of Molecular Therapeutics and Formulation, Boots Science Building, School of Pharmacy, University of Nottingham, Nottingham, NG7 2RD, UK. E-mail: cameron.alexander@nottingham.ac.uk
[b]Biodiscovery Institute, School of Medicine, University of Nottingham, Nottingham, NG7 2UH, UK
[c]Department of Pharmaceutical Biotechnology, Faculty of Pharmacy, Hacettepe University, Ankara 06100, Türkiye
[d]Warsaw University of Technology, Faculty of Chemistry, Noakowskiego 3 St., 00-664 Warsaw, Poland
[e]Department of Haematology, UCL Cancer Institute, 72 Huntley Street, University College London, London, WC1E 6DD, UK
[f]Department of Medical Biology, Faculty of Medicine, Izmir Bakircay University, Izmir, Türkiye
[g]Department of Medical Pharmacology, Faculty of Medicine, Izmir Bakircay University, Izmir, Türkiye
[h]UCL School of Pharmacy, University College London, 29-39 Brunswick Square, Bloomsbury, London, WC1N 1AX, UK. E-mail: p.gurnani@ucl.ac.uk

cytosol.[5,6] These delivery systems are typically nanoparticle-based materials, such as lipid nanoparticles (LNPs), which have been clinically used for three approved nucleic acid products (Onpattro, Spikevax and Comirnaty).[7] However, their chemical versatility and limited intellectual property space create an urgent need for alternative delivery systems. Among these, polycations are recognised as a potent but clinically immature delivery approach.[8,9] These systems operate by condensing negatively charged mRNA into small (50–200 nm) polyplex nanoparticles with positively charged cationic polymers through opposing electrostatic interactions.[10,11] One promising subclass is poly(beta-amino esters) (PBAEs), which contain hydrolysable ester bonds in their backbone, enabling biodegradability and facilitating RNA release.[12–14] Their highly tunable chemistry supports adaptation to different nucleic acid cargos, making them strong candidates for RNA delivery.[15–17] In addition to their delivery capacity, certain PBAEs can influence immune responses, providing a platform that can be further tailored with immunostimulatory components.[18] The significantly broader chemical versatility of these materials makes them ideal systems for improving the immune response of mRNA vaccines.

In principle, messenger RNA vaccines and immunotherapies display self-adjuvanting behaviour due to the agonist properties of exogenous RNA on endosomal (Toll-like receptor 7/8) and cytosolic (RIG-I, MDA-5) single-stranded RNA sensors, which mimic the inflammatory process of an infective RNA virus.[19,20] However, the condensation of mRNA into nanoparticles and the use of modified nucleotides, such as 1-methylpseudouridine (m1ψ), hinder the activation of these processes in antigen-presenting cells (APCs), weakening the initial steps of the adaptive immune response.[21] However, the excessive activation of these inflammatory processes simultaneously puts APCs into an 'anti-proliferative' state, thus shutting down the protein synthesis machinery of the cells and reducing the translation efficiency of the delivered mRNA construct.[21,22]

Traditional vaccines and immunotherapies achieve a robust immune response by utilising adjuvants and immunostimulatory molecules, which are co-formulated with the active ingredient.[23] Adjuvanticity can be introduced either from a humoral immunity perspective, through controlled release of the antigen, or preferably through direct activation of cellular immunity through the co-formulation of molecules, which simulates the natural infection process by binding to pathogen recognition receptors (PRRs) at the immune cell surface.[24] Key examples of these are agonists for Toll-like receptors (TLRs), a specific PRR class found in APCs, macrophages and other cells, which, when stimulated, elicit downstream expression of pro-inflammatory cytokines that form the innate immune response.[25]

The development of adjuvanted mRNA formulations, which co-deliver the antigen encoding nucleic acid and adjuvant to the same cells, could therefore represent a powerful strategy to strengthen and broaden the immune response of mRNA vaccines while providing a flexible platform to mitigate any inflammation-induced inhibition of mRNA translation.[26,27] There is significant evidence that LNP formulations display intrinsic adjuvanticity, but these effects are not always predictable and are dependent on cationic/ionisable lipid structures.[28,29] In contrast, there has been significant progress in targeted adjuvant formulations for mRNA vaccines and therapies, often through the co-formulation or conjugation of TLRa's, such as polyinosine-cytosine (polyI:C, TLR3a), imidazoquinolines (TLR7/8a) and CG-rich oligonucleotides (CpG-ODN, TLR9a) from an LNP perspective.[30–32] Meanwhile, the few limited reports of adjuvanted polycation delivery systems focus on the co-formulation of polyI:C and CpG-ODNs; however, to the best of our knowledge, direct conjugation of a TLR agonist adjuvant has not been reported for polymer-based mRNA formulations.[33,34]

Herein, we report the development of a TLR7a-conjugated polycation as a potential adjuvanted formulation for mRNA and self-amplifying mRNA, an mRNA technology that includes replicase genes, amplifying the construct within the cytosol. saRNAs can therefore enhance protein expression levels at significantly lower doses, lengthening the expression half-life and reducing the cost compared to mRNA.[35,36] We utilised the intrinsic chemistry of Loxoribine (a guanosine analogue known as a TLR7 agonist) to conjugate it to the end-groups of a PBAE cationic polymer, which is a well-established polymeric delivery system for mRNA and saRNA modalities. The Loxoribine–PBAE conjugate was then formulated with saRNA to form adjuvanted polyplexes, which were characterised for their delivery efficiency, transfectability and ability to stimulate the TLR7 pathway in cells. Finally, the polyplexes were further evaluated in bone marrow dendritic cell (BMDC) experiments to assess dendritic cell activation (Fig. 1).

Materials and methods

Materials

1,4-Butanediol diacrylate (BDD), 5-aminopentan-1-ol (5-AP), 2,2′-(ethylenedioxy)bis(ethylamine), 3-mercaptopropanyl-*N*-hydroxysuccinimide ester, tris(2-carboxyethyl)phosphine (THP), triethylamine (TEA), fluorescein isothiocyanate (FITC), diethyl ether, tetrahydrofuran, sodium acetate (NaOAc) buffer (pH: 5.0) and the dye Gel Red were purchased from Sigma-Aldrich. Loxoribine was purchased from InvivoGen. Dichloromethane (DCM), *N*,*N*-dimethylformamide (DMF), acetonitrile (ACN), tetrahydrofuran (THF), hexane, diethyl ether, dimethyl sulfoxide (DMSO), loading buffer, Tris-acetate-EDTA (TAE) buffer, tris-(2-hydroxyethyl) phosphine (THP), Lipofectamine Messenger MAX™, Hoechst 33342, Lysotracker red and 96-well plates were obtained from ThermoFisher Scientific. Dulbecco's Modified Eagle's medium (DMEM), RPMI 1640 cell culture medium, HEK-Blue Detection medium, fetal bovine serum (FBS) and Opti-MEM were bought from Gibco, Invitrogen, Carlsbad, CA, USA. PrestoBlue reagent and ONE-Glo D-luciferin substrate were purchased from Promega, UK. Self-amplifying RNA was synthesised as previously described.[35] mRNA was purchased from TriLink Biotechnologies.

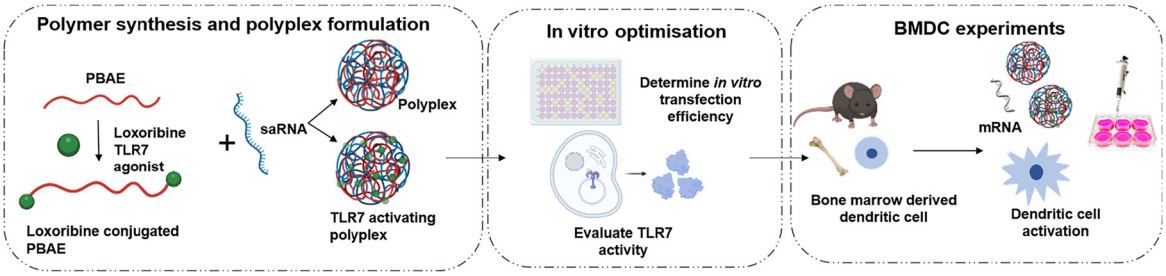

Fig. 1 Schematic of the PBAE synthesis, polyplex assembly, analysis of *in vitro* transfection and toxicity profiles, and evaluation of TLR7 activation and bone marrow dendritic cell (BMDC) experiments to assess dendritic cell activation.

Instrumentation and analysis

NMR spectroscopy. All ^{1}H-NMR spectra were recorded in ppm (δ) at 400 MHz in d6-DMSO using a Bruker Avance III MHz spectrometer maintained at 25 °C. To analyse the spectra, MestReNova 6.0.2 copyright 2009 (Mestrelab Research S.L.) was applied.

Gel permeation chromatography. Gel permeation chromatography (GPC) analysis was performed using the PL-50 instrument equipped with a dual angle light scatter (LS), viscometry (VS) and differential refractive index (DRI). The system was equipped with a PLgel 5 µm guard column and a 2 × PLgel Mixed D column (300 × 7.5 mm). Dimethylformamide (DMF) with LiBr (0.1% wt/wt) was utilised as the eluent with a flow rate of 1 mL min^{-1} at 50 °C. The instrument was calibrated with poly(methyl methacrylate) standards (Agilent EasyVials) in the range of 955 500–550 g mol^{-1}. Using conventional calibration and Cirrus GPC software, dispersity ($Đ$) values, molecular weight (M_w) and experimental molar mass (M_n, SEC) were determined.

DLS and zeta potential. A Zetasizer nano-ZS90 (Malvern, Inc.) dynamic light scattering (DLS) instrument was used to characterise the particles in terms of their size, polydispersity index (PDI) and zeta potential. The instrument was used at 25 °C to determine the zeta potential, average hydrodynamic diameter, and PDI of the polyelectrolyte complexes.

Transmission electron microscopy. Briefly, glow-discharged Formvar/carbon-coated TEM grids were used, on which the formulation samples (13 µL) were placed and left for 15 minutes. Then, the excess solution was removed, and the samples were allowed to dry at room temperature. Following this, 10 µL of 2% aqueous uranyl acetate was applied to each grid and left for 10 seconds. After air drying, imaging was performed using a Tecnai G2 Spirit TEM with a BioTwin lens configuration (Thermo Fisher Scientific, Eindhoven, The Netherlands) at an accelerating voltage of 100 kV.

Polymer synthesis and characterisation

pBDD-5AP. To BDD (1000 mg, 5 mmol) in DMSO (0.95 mL), 5-AP (470 mg, 4.56 mmol) in DMSO (2 mL) was added, and the reaction mixture was stirred at 90 °C overnight. Then, the mixture was diluted with THF (2.94 mL), the product was isolated by precipitation from diethyl ether (40 mL), and further purified by redissolving in THF (3 mL) and precipitation in diethyl ether (40 mL) thrice. The product was dried under vacuum overnight, yielding 1250 mg (85%) of a yellowish oil. The molecular weights were determined by SEC (M_n = 6.2 kDa, M_w = 8.0 kDa, and $Đ$ = 1.3); for ^{1}H NMR, see Spectrum S1 in the SI.

H_2N-(pBDD-5AP)-NH_2. To produce amine end-capped PBAEs, an excess amount of 2,2′-(ethylenedioxy)bis(ethylamine) (300 mg, 2.02 mmol) was added to the BDD-5AP (1000 mg) in DMSO (10 mL) in a 20 mL vial, and the mixture was stirred for 24 hours at room temperature. Polymers were isolated by diluting the reaction mixture with THF (10 mL), followed by dropwise precipitation in diethyl ether (40 mL) thrice. The polymer was collected *via* centrifugation and dried under reduced pressure at 37 °C, and a yellow viscous liquid was obtained. Finally, the polymers were stored at −20 °C as a 100 mg mL^{-1} solution in DMSO. Molecular weights were determined by SEC (M_n = 6.6 kDa, M_w = 9.1 kDa, $Đ$ = 1.4); for ^{1}H NMR, see Spectrum S2 in the SI.

SH-(pBDD-5AP)-SH. To produce SH-end-capped PBAEs, an excess amount of mercaptopropanyl-*N*-hydroxysuccinimide ester (84.5 mg, 0.42 mmol) was added to H_2N-(pBDD-5AP)-NH_2 (500 mg) in DMSO (5 mL) in a 20 mL vial. Then, TEA (16.8 mg, 0.16 mmol) and THP (2.5 mg, 20 µmol) were added to the mixture. The mixture was stirred for 3 hours at room temperature under argon and UV light to avoid polymer crosslinking. Polymers were isolated by diluting the reaction mixture with THF (5 mL), followed by dropwise precipitation in diethyl ether (40 mL) thrice. The polymer was collected *via* centrifugation and dried under reduced pressure at 37 °C, and a yellow viscous liquid was obtained. Finally, the polymers were stored at −20 °C as a 100 mg mL^{-1} solution in DMSO. Molecular weights were determined by SEC (M_n = 6.9 kDa, M_w = 9.9 kDa, $Đ$ = 1.4); for ^{1}H NMR, see Spectrum S3 in the SI.

LOX-(pBDD-5AP)-LOX. Finally, to obtain LOX-end-capped PBAEs, an excess amount of Loxoribine (141 mg, 0.41 mmol) was added to HS-(pBDD-5AP)-SH (500 mg) in DMSO (5 mL) in a 20 mL vial. Then, TEA (16.8 mg, 166 µmol) and THP (2.5 mg) were added to the mixture. The mixture was stirred for 3 hours at room temperature under argon and UV conditions to avoid polymer crosslinking. Then, the mixture was dialysed (3.5 kDa molecular weight cut-off) against DMSO (1 L) for 24 hours, and the DMSO solution was changed once. Afterwards, the mixture was precipitated in diethyl ether (40 mL), and to

remove the remaining DMSO, it was redissolved in THF (5 mL) and precipitated in diethyl ether (40 mL) thrice. The product was dried under a vacuum overnight, and a dark yellowish viscous liquid was obtained. Molecular weights were determined by SEC (M_n = 7.8 kDa, M_w = 11 kDa, $Đ$ = 1.4); for ^{1}H NMR, see Spectrum S4 in the SI.

Synthesis of fluorescently labelled polymers. LOX-(pBDD-5AP)-LOX polymer was dissolved in 5 mL DMSO (0.5 mg ml^{-1}) in a 20 mL vial. FITC was added to the vials at a 1 : 10 (moles of end amine : FITC) molar ratio, and TEA was added to the mixture at a 0.1 molar ratio. The reaction mixture was stirred for 24 hours in the dark at room temperature. The reaction mixture was then dialysed in the dark using a 3.5 kDa molecular weight cut-off against 250 mL NaOAc buffer (pH: 5.0). Purification was continued for 4 days, and the dialysis medium was refreshed 2 times a day. After freeze drying, the FITC-labelled polymers were collected as a yellow solid and stored at −20 °C as a 100 mg mL^{-1} solution in DMSO.

Polymer buffering capacity assay. The buffering capacity of the polymers was evaluated by acid–base titration over a pH range of 10.0–3.0. Briefly, 2 mg of the polymer was dissolved in 30 mL of 0.1 M NaCl aqueous solution, and the solution was adjusted to pH 10.0 using 0.1 M NaOH. Then, precise volumes (in the range of 20–40 μL) of 0.1 M HCl were added until a pH of 3 was achieved. The pH was recorded after each addition of HCl. 0.1 M NaCl was used as the negative control.

Preparation of polyplexes

Polyplexes were prepared by electrostatic interactions between positively charged polymers and negatively charged saRNA or mRNA by mixing various w/w ratios (32, 64 and 128). First, the working dilutions of the polymers and saRNA or mRNA were prepared in 25 mM NaOAc buffer (pH: 5.0). Depending on the desired w/w ratio, different amounts of polymer stock solutions (100 mg mL^{-1} in DMSO) were mixed with nucleic acids in the buffer, gently mixed using a pipette and incubated at room temperature for 30 minutes. Although preparing the PBAE/saRNA complexes, taking a w/w 64 ratio as an example, 10 μg mL^{-1} of the RNA stock solution was mixed with 2.560 mg mL^{-1} PBAE by pipetting using a 25 mM NaOAc buffer.

Encapsulation efficiency using a RiboGreen assay

A fluorescence-based Quant-iT RiboGreen assay (ThermoFisher, UK) was utilised to detect free RNA in the solution after polymer encapsulation. Samples were diluted in 1× TE buffer (v/v 1 : 1), and the assay was performed according to the manufacturer's protocol. Samples were then loaded on a black 96-well plate and analysed for fluorescence using a microplate reader at an excitation of 485 nm and emission at 528 nm.

Determination of drug loading

The evaluation of Loxoribine amount in LOX-(pBDD-5AP)-LOX nanoparticles was conducted through high-performance liquid chromatography (HPLC) quantification. Initially, 1 mg of the LOX-end-capped formulation was suspended in 1 mL of 1 M HCl and subjected to 4-hour incubation at 37 °C to facilitate nanoparticle degradation and release of the therapeutic agent. Subsequently, the drug content was analysed using a Shimadzu UFLC system (Shimadzu Corporation, Kyoto, Japan) equipped with a Hichrom 5 C18 column (250 × 4.6 mm) at room temperature. The mobile phase, composed of water and acetonitrile in a 20 : 80 ratio, flowed at 1 mL min^{-1}. A 20 μL injection volume was used, and the drug was monitored at 254 nm. Loxoribine exhibited a retention time of 2 minutes. The method demonstrated linear responses within a concentration range of 0.6–200 μg mL^{-1}. The results are presented as the mean ± standard deviation (SD). The drug loading was calculated using the following equation:

$$\text{Drug load}\,(\%) = \frac{\text{weight of drug}\,(\text{mg})}{\text{weight of formulation}\,(\text{mg})} \times 100.$$

Determination of drug loading using ultraviolet–visible spectroscopy

To assess the drug loading efficiency of the polymer formulations, UV-Vis spectroscopy was employed. Polymers were dissolved in 25 mM sodium acetate (NaOAc) buffer (pH 5.0) at a concentration of 1 mg mL^{-1}, ensuring complete solubilization. Serial dilutions of Loxoribine (ranging from 3 to 100 μg mL^{-1}) were also prepared using the same buffer to generate a standard calibration curve.

All solutions were transferred into quartz cuvettes and subjected to UV-Vis spectral analysis using a Tecan Spark spectrophotometer. Absorbance measurements were recorded at λ_{max} = 251 nm and 300 nm, which correspond to the characteristic absorption peaks of Loxoribine. The drug loading was determined by comparing the absorbance values of the polymer-loaded drug solutions to the standard calibration curve.

In vitro experiments

Cell culture. Human embryonic kidney 293T (HEK293T) cells were a gift from Imperial College London and cultured in 10% (v/v) FBS containing high glucose DMEM. DC2.4 cells were obtained from ATCC and cultured in RPMI 1640 cell culture medium. Media containing L-glutamine was supplemented with 4-(2-hydroxyethyl)-1-piperazineethanesulfonic acid (10 mM), non-essential amino acids (0.1 mM) and 10% FBS. Human TLR7-transfected HEK cells (HEK-Blue™) were purchased from InvivoGen and cultured in 10% (v/v) FBS containing high glucose DMEM. The absence of mycoplasma was confirmed using a polymerase chain reaction. The cells were grown to 90% confluence in a humidified incubator at 37 °C (5% CO2) and detached with 1× trypsin/EDTA. Viability was assessed using Trypan Blue staining.

Cell viability assays. To investigate the cytotoxicity of the formulations, a cell viability assay was performed in the HEK293T, DC2.4 and HEK-BLUE cell lines. 24 hours prior to treatment, cells were seeded in a clear 96-well plate at a density of 20 × 10^3 cells per well. For the treatment, the medium was aspirated, and the cells were treated with 200 μL of Opti-MEM containing various w/w ratios of formulations complexed with 10 μg mL^{-1} fluc saRNA concentration (20 μL of polyplex solution). After

4 hours, the nanoparticles were aspirated, and 100 μL of complete medium was added to the wells. At 24 hours post-treatment, each well was treated with 100 μL of 10% PrestoBlue reagent and allowed to incubate for 1 hour. Then, the total volume was transferred to a black 96-well plate, and the FLUOstar Omega plate reader (BMG LABTECH, UK) was used to determine the fluorescent intensity (540–590 nm) of each well and normalized to the medium control.

***In vitro* transfection experiments.** *In vitro* transfection experiments were performed in HEK293T and DC2.4 cell lines, and the commercially available transfection reagent Lipofectamine Messenger MAX™ was used as a positive control. 24 hours prior to treatment, cells were seeded in a clear 96-well plate at a density of 20×10^3 cells per well. For the treatment, the medium was aspirated; then, the cells were transfected with 200 μL of Opti-MEM containing various w/w ratios of formulations complexed with 10 μg mL^{-1} fluc saRNA concentrations (20 μL of polyplex solution). After 4 hours, the nanoparticles were aspirated, and 100 μL of medium was added to the wells. At 24 hours post-treatment, 50 μL of media was removed. Then, 50 μL of the ONE-Glo D-luciferin substrate was placed into each well and mixed well by pipetting. Finally, the total 100 μL was placed in a 96-well plate, and the FLUOstar Omega plate reader (BMG LABTECH, UK) was used to determine the luminescence.

TLR7 activation assay. TLR7 activation was tested on human TLR7-transfected HEK cells (HEK-BLUE). The commercially available transfection reagent Lipofectamine Messenger MAX™ was used as a positive control. 24 hours prior to treatment, cells were seeded in a clear 96-well plate at a density of 20×10^3 cells per well. For the treatment, the medium was aspirated; then, cells were transfected with 200 μL of HEK-Blue Detection medium containing polymers only (without saRNA, 20 μL) with different w/w ratios and various w/w ratios of formulations complexed with 10 μg mL^{-1} fluc saRNA concentrations (20 μL of polyplex solution). At 24 hours post-treatment, absorbance was measured at 620 nm using a FLUOstar Omega plate reader (BMG LABTECH, UK).

Cellular uptake of saRNA USING CONFOCAL MICROSCOPY. HEK293T and DC2.4 cells were seeded in CellView™ 35 mm diameter glass bottom cell culture dishes at a density of 30×10^4 cells per well. For the treatment, the medium was aspirated, and the cells were transfected with Opti-MEM containing FITC-labelled LOX-end-capped formulation (LOX-(pBDD-5AP)-LOX) w/w 128 at 0.01 mg mL^{-1}. The cells were incubated for 2 hours at 37 °C with 5% CO2. Then, nanoparticles were aspirated, and cells were washed 3 times with PBS and stained with 10 μg mL^{-1} Hoechst 33342 and 75 nM Lysotracker red applied in PBS solution. After 30 minutes, the solution was aspirated, and cells were washed 3 times with PBS; then, FluoroBrite DMEM was added to the cells. Imaging was performed using Leica confocal microscopy with LAS X software on DAPI, FITC and Lysotracker filters. ImageJ software was used to process the pictures.

Imaging flow cytometry. DC2.4 cells were seeded in a clear 6-well plate at a density of 40×10^5 cells per well. For the treatment, the medium was aspirated, and the cells were transfected with an Opti-MEM containing LOX-(pBDD-5AP)-LOX w/w 128 (0.01 mg mL^{-1}) formulation. After 4 hours, nanoparticles were aspirated, and 150 μL of 0.05% trypsin was used for the detachment of cells from wells. After incubation for 15 minutes, 300 μL FACS buffer was used to neutralise the trypsin, and the cells were centrifuged at 1500 rpm for 10 minutes. Following this, the cells were stained with Zombie Violet (1 : 500) dye for 30 minutes at room temperature in order to help with gating on live cells. Then, the cells were fixed with 100 μL of 4% paraformaldehyde in PBS for 20 minutes. Fixed cells were centrifuged, and pellets were resuspended in 50 μL of PBS. Data were acquired using ImageStream 100 (Amnis, Seattle, US), and on single cell in focus events was used for the analysis. Ideas Software (Amnis, Seattle, WA, USA) was used for the data analysis. Total cell fluorescence was calculated by default using total cell masks for the measurement of nanoparticle internalisation, and cell interiors were identified using the area erode tool (brightfield channel). The internalisation index was shown as a percentage of maximum internalisation (percentage of interior cell fluorescence to total cell fluorescence).

***In vitro* bone marrow dendritic cell (BM DC) transfection experiments.** C57BL/6 female mice were purchased from Charlie River, UK. *In vivo* femurs and tibias were collected from 6- to 12-week-old C57BL/6 female mice, and bone marrow cells were released by mortar and pestle in complete RPMI media. Red blood cells were lysed with ACK lysis buffer and washed with complete media. The remaining progenitor cells were plated 2×10^6 cells per mL in a 24-well non-tissue culture-treated plate with 150 ng mL^{-1} Flt3-L. On day 8, BM DCs were transfected with polyplexes at 1 μg mL^{-1} mRNA and 128 μg mL^{-1} PBAE concentrations and left for 24 h of incubation. On day 9, cells were harvested and labelled for surface staining, as detailed in SI Table S1. Flow cytometer data were collected using a Fortessa instrument and analysed using FlowJo software Version 10.

Statistical analysis

Graphs and statistics were prepared in GraphPad Prism 9.5.1 version or higher. Statistical differences were analysed using either one-way or two-way ANOVA adjusted for multiple comparisons (either Tukey's or Dunnett's). A p value lower than 0.05 was considered statistically significant, and the levels of statistical significance were set to $p^* < 0.05$, $p^{**} < 0.01$, $p^{***} < 0.001$ and $p^{****} < 0.0001$.

Results and discussion

Synthesis and characterisation of PBAEs

A synthetic pathway consisting of four steps was employed to synthesise the targeted poly(beta amino ester) (PBAE), modified covalently with TLR7 agonist Loxoribine (Fig. 2A). In the first step, 1,4-butanediol diacrylate (BDD) was reacted with 5-aminopentanol (5AP) using a molar excess of BDD to yield a

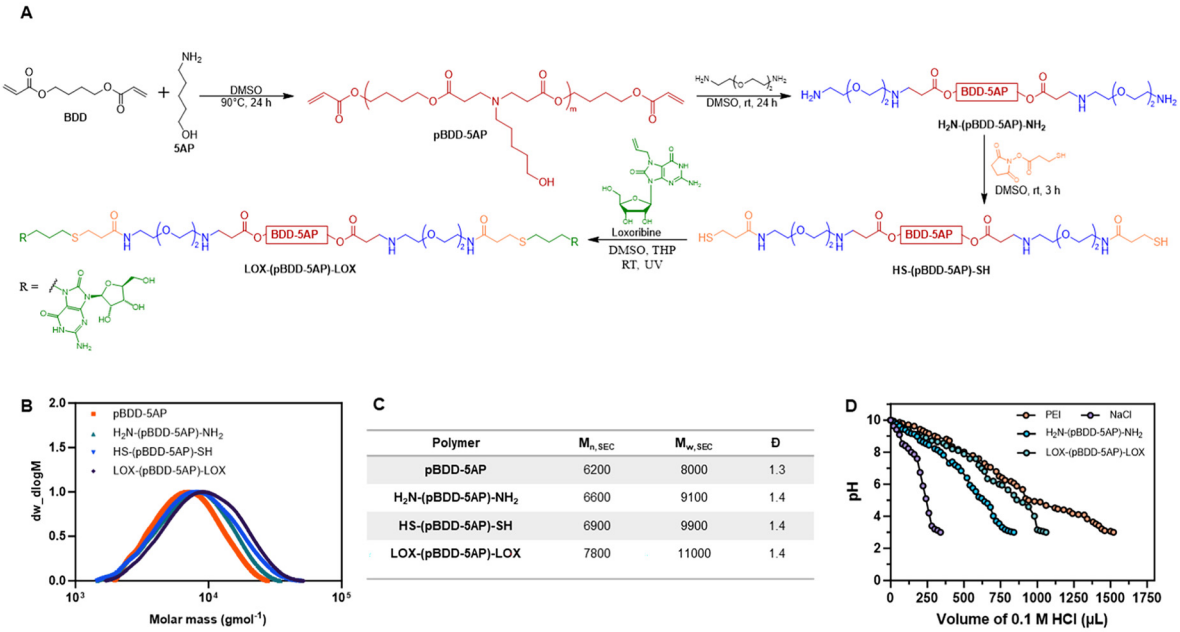

Polymer	$M_{n,SEC}$	$M_{w,SEC}$	Đ
pBDD-5AP	6200	8000	1.3
H_2N-(pBDD-5AP)-NH_2	6600	9100	1.4
HS-(pBDD-5AP)-SH	6900	9900	1.4
LOX-(pBDD-5AP)-LOX	7800	11000	1.4

Fig. 2 Synthesis and characterisation of PBAEs. (A) Synthetic scheme for the step-growth Michael-addition polymerisation of BDD and 5-AP, followed by end-capping with 2,2′-(ethylenedioxy)bis(ethylamine) and 3-mercaptopropanyl-*N*-hydroxysuccinimide ester to produce LOX-end-capped PBAE (Step 4). (B) Molecular weights of PBAEs determined using GPC, and (C) molecular weight distribution of pBDD-5AP, H_2N-(pBDD-5AP)-NH_2, SH-(pBDD-5AP)-SH and LOX-(pBDD-5AP)-LOX. (D) Buffering capacity of H2N-(pBDD-5AP)-NH_2 and LOX-(pBDD-5AP)-LOX compared with polyethyleneimine (PEI) and a 0.1 M NaCl(aq) solution as the negative control.

PBAE terminated with the acrylic group, pBDD-5AP. This PBAE was chosen due to previous preclinical studies, showing high mRNA transfection capability both *in vitro* and *in vivo*.[37] The successful synthesis of the acrylic-terminated PBAE, pBDD-5AP, was confirmed using ^{1}H NMR spectroscopy, as signals around 6.3–5.9 ppm on the ^{1}H NMR spectrum indicated the presence of double bonds (Spectrum S1). p(BDD-5AP) was then end-capped with 2,2′-(ethylenedioxy)bis(ethylamine) *via* a further aza-Michael addition reaction to yield the amine-terminated PBAE H_2N-(pBDD-5AP)-NH_2, which was confirmed, as the ^{1}H NMR spectrum indicated the complete disappearance of acrylic end-groups (Spectrum S2). H_2N-(pBDD-5AP)-NH_2 was further transformed with *N*-hydroxysuccinimidyl-3-mercaptopropanoate to yield the thiol end-capped PBAE HS-p(BDD-5AP)-SH polymer. The success of this modification was proven by the appearance of two signals characteristic of the 3-mercaptopropionate group: at 2.90 ppm from the alpha-methylene group of the thiol moiety and at 2.20 ppm from the thiol group (Spectrum S3). The thiol groups were then used as a reactive handle to conjugate Loxoribine to the PBAEs, which contain a double bond, making them suitable for thiol–ene chemistry under UV irradiation, leading to the final product LOX-p(BDD-5AP)-LOX. Due to difficulties with the analysis of an NMR spectrum of the final product, as a small molecule was conjugated with the polymer (Fig. 2), successful conjugation with Loxoribine was demonstrated using HPLC and UV-Vis spectroscopy experiments (see SI, Fig. S3). These methodologies allowed the determination of the total content of Loxoribine in the final polymer, which was found to be approximately 27 µg per mg PBAE (w/w 2.7%). All intermediate products and the final product were characterised by means of GPC (Fig. 2B and C), where the molar mass was observed to increase after each end modification step (6200, 6600, 6900 and 7800 g mol^{-1}), and monomodal chromatograms with around $Đ$ = 1.4 were revealed. The buffering capacities were assessed for H_2N-(pBDD-5AP)-NH_2 and LOX-(pBDD-5AP)-LOX, as the pK_a of polycations has been recognised as crucial for enhancing endosomal buffering and endo/lysosomal escape of polymer-based nucleic acid delivery systems (Fig. 2D). Acid–base titration in the pH range of 10.0–3.0 for amine-end-capped PBAE titration curve was observed between the negative control (NaCl) and the positive control (PEI). However, with LOX-end-capped PBAE, the titration curve was similar to that of PEI, indicating that LOX-end-capping increased their buffering capacity (Fig. 2D) likely due to the purine rings of LOX even though only 2 drug molecules were added to each polymer chain.

Polyplex physicochemical properties of different end-capped polyplexes

Polyplex preparation was performed at three different polymer/fluc saRNA weight-to-weight ratios (w/w ratios of 32, 64 and 128) for H_2N-(pBDD-5AP)-NH_2 and LOX-(pBDD-5AP)-LOX PBAEs. Solutions of saRNA and the polymers were prepared using 25 mM NaOAc buffer; then, the nucleic acid solution was dropwise added to the polymer solution at a 1 : 1 volume ratio using a pipette. The prepared nanoparticles were incubated at room temperature for 30 minutes prior to use.

Experiments were then performed to define the physicochemical and biological characteristics of the polyplexes, encompassing particle size, surface charge, encapsulation efficiency, biocompatibility, and RNA expression (see Fig. 3A).

Hydrodynamic diameters of all nanoparticles were observed to be in the range of 100–200 nm with low polydispersity index (PDI) values (<0.2) determined by dynamic light scattering (DLS) (Fig. 3B), with no major changes in particle size observable across different w/w ratios. Notably, the LOX-(pBDD-5AP)-LOX polyplexes were larger than the H_2N-(pBDD-5AP)-NH_2 polyplexes, suggesting that end modification of the polymer with LOX affected the structures of the polyplexes. We reasoned that this could be due to the removal of the free NH_2 end groups to the more bulky but possibly less protonated (at ambient pH) purine groups of LOX, which changed the sterics and electrostatics of the complexation interactions with RNA. However, the hydrodynamic diameters of LOX-(pBDD-5AP)-LOX polyplexes were significantly decreased with increasing w/w ratios possibly due to the increased cation content that can induce more compact structures, which is consistent with previous reports on polyplexes.[38]

Next, the zeta potentials of the particles were measured using DLS. Notably, higher zeta potential values were revealed for LOX-(pBDD-5AP)-LOX polyplexes (24 ± 8 mV) compared to H_2N-(pBDD-5AP)-NH_2 (20 ± 2 mV), which could be due to the addition of LOX, as mentioned above due to the purine rings of LOX and increased surface-exposed charges on the polyplexes (Fig. 3C). The encapsulation efficiency of nanoparticles was analysed utilizing a RiboGreen assay and showed full RNA encapsulation for all nanoparticles produced at all ratios (Fig. 3D). Finally, TEM micrographs of all polyplexes prepared at a w/w ratio of 128 indicated mostly spherical complexes from 25 to 280 nm in diameter, which is consistent with DLS analysis, and allowed for some particle shrinking during dehydration for TEM (Fig. 3E). Furthermore, as DLS analysis can overrepresent larger particles present in heterogeneous particle distributions, it is likely that any smaller species visible by TEM may not have been included in the particle size averages.[39] TEM images are intended for qualitative visualisation; apparent aggregation may result from negative staining and may not fully reflect the native nanoparticle structure. Overall, these results indicate that all six polyplexes were capable of encapsulating saRNA and producing particle sizes below the typical 200 nm diameter threshold for efficient gene delivery.

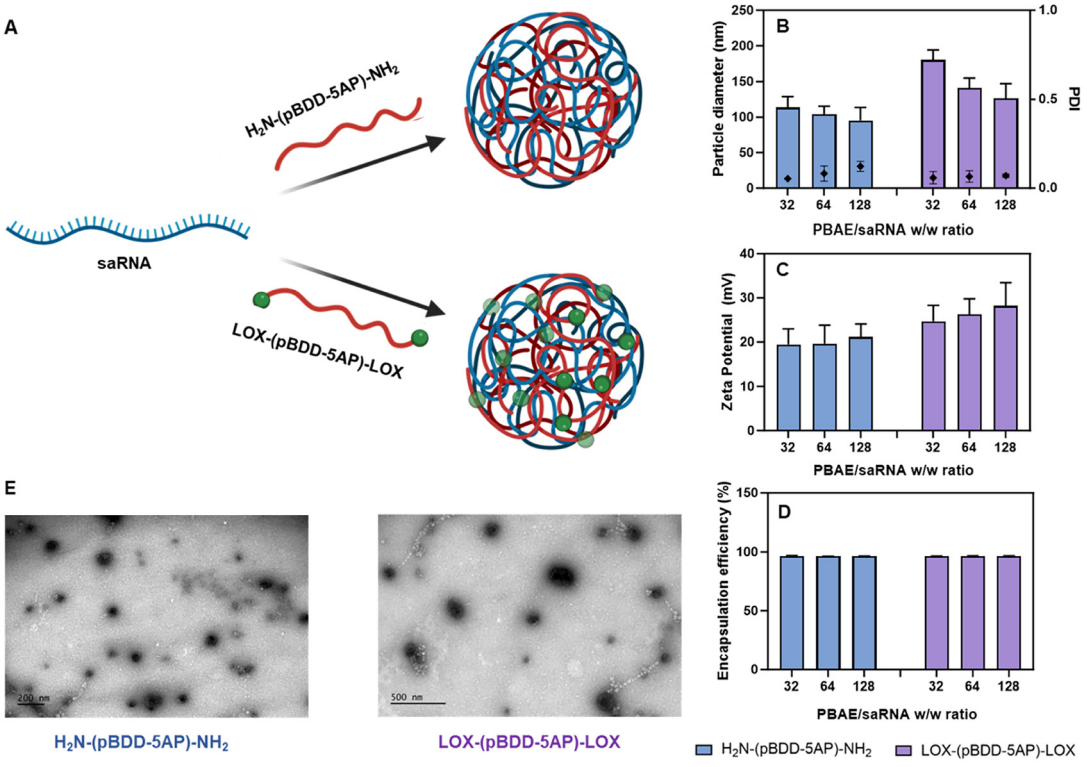

Fig. 3 Formulation of PBAEs with saRNA to produce polyplex nanoparticles. (A) Schematic of saRNA formulation with H_2N-(pBDD-5AP)-NH_2 and LOX-(pBDD-5AP)-LOX prepared in 25 mM sodium acetate pH 5.0 at a final saRNA concentration of 10 μg mL^{-1}. (B) Particle size and (C) zeta potential for the H_2N-(pBDD-5AP)-NH_2 and LOX-(pBDD-5AP)-LOX polyplexes at a PBAE/saRNA w/w ratio of 32, 64 and 128 determined by dynamic light scattering at 25 °C. Bars represent the mean ± SD. (D) Encapsulation efficiency of saRNA within polyplexes evaluated using the RiboGreen assay. Bars represent the mean ± SD. (E) Representative transmission electron micrograph of the polyplexes H_2N-(pBDD-5AP)-NH_2 and LOX-(pBDD-5AP)-LOX. All data are presented as mean ± SD, with $n = 3$ for all conditions. Statistical significance was determined using a two-way ANOVA test, with $P < 0.05$ considered significant.

In vitro evaluation of RNA delivery

Transfection and metabolic activity of different end-capped polyplexes. The acute toxicity and saRNA delivery efficiency of individual formulations H_2N-(pBDD-5AP)-NH_2 and LOX-(pBDD-5AP)-LOX were evaluated in HEK293T cells (as a model cell line) and DC2.4 cells (a relevant dendritic cell line for vaccines). Similar to the formulation characterisation study described earlier, polyplexes were prepared at polymer/saRNA w/w ratios of 32, 64, and 128 using firefly luciferase encoding saRNA. The resulting polyplexes were compared with Lipofectamine (the positive expression control) and Triton X-100 (the positive toxicity control).

All formulations demonstrated higher viability values (over 80% as inferred from metabolic activity) compared to the positive control Lipofectamine (50%) (Fig. 4A and B). It can be

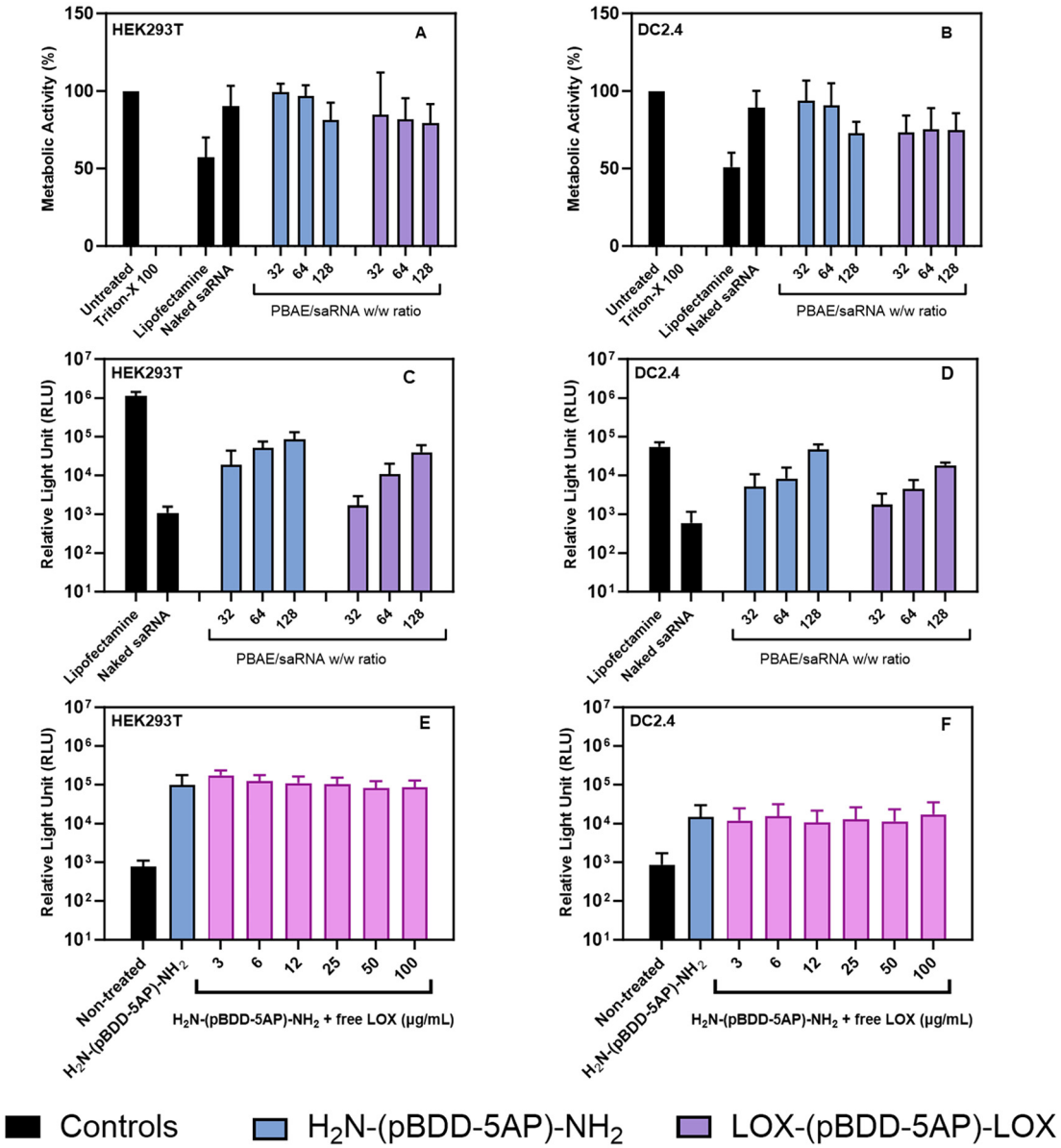

Fig. 4 Metabolic activity and transfection efficiency of PBAE-derived saRNA polyplexes. Effect of PBAE polyplexes formulated with firefly luciferase-encoding saRNA at PBAE/saRNA w/w ratios of 32, 64 and 128 on metabolic activity (A and B) and transfection efficiency (C and D) on HEK293T cells (A and C) and DC2.4 cells (B and D). The cells were treated with polyplexes containing saRNA at a concentration of 500 ng mL^{-1} (100 ng per well) in serum-free Opti-MEM. Metabolic activity was compared with Triton X (positive control) and untreated cells (negative control) and was calculated by normalizing metabolic activity to untreated cells. *In vitro* transfection efficiency was analysed 24 h post-transfection using the Promega ONE-GLO luciferase assay and compared with Lipofectamine Messenger MAX™ (positive control) and naked saRNA (negative control), expressed as relative light units (RLU) for luciferase expression. (E and F) RLU for H_2N-(pBDD-5AP)-NH_2 and H_2N-(pBDD-5AP)-NH_2 + free LOX dilutions (3–100 μg mL^{-1}) in HEK293T and DC2.4 cells. Bars represent the mean ± SD. All data are presented as mean ± SD, with n = 3 for all conditions. Statistical significance was determined using a two-way ANOVA test, with $P < 0.05$ considered significant.

implied that the conjugation of Loxoribine did not affect the metabolic activity in these cell lines. Similar to previous studies, increasing w/w ratios of H_2N-(pBDD-5AP)-NH_2 resulted in increased toxicity due to increased polycation concentration, which is known to disrupt the negative phospholipid bilayer[40,41] (Fig. 4A). Interestingly, no substantial difference was detected for the LOX-(pBDD-5AP)-LOX formulations despite the increasing w/w ratios. In terms of transfection efficiency, in general, saRNA expression was slightly lower for the LOX-(pBDD-5AP)-LOX formulations compared to the amine end-capped analogues (Fig. 4C and D). This could be due to the above-mentioned slightly larger nanoparticle diameters of the LOX-end-capped formulations, where the cellular uptake could be lower. Notably, increasing w/w ratios of the formulations in both cell lines resulted in higher transfection.[42] In HEK293T cells, the transfection efficiencies of the w/w ratio 128 were lower than Lipofectamine; however, in CD2.4 cells, both formulations (w/w 128) showed high transfection efficiency as the positive control.

Given the lower transfection efficiencies of the Loxoribine-conjugated PBAE in both HEK293Ts and DC2.4s, we wanted to evaluate whether the co-incubation of free Loxoribine caused the same effect. To decouple the effect of Loxoribine from polymer end-group modification, cells were treated with amine-end-capped PBAE/saRNA polyplexes (w/w 128) in the presence of increasing concentrations of free Loxoribine (0–100 μg mL^{-1}), covering the LOX-equivalent range present in LOX-(pBDD-5AP)-LOX formulations, and compared to naked saRNA controls (Fig. 4E and F). Loxoribine addition at all concentrations did not significantly influence transfection efficiency in both HEK293Ts and DC2.4s. This contrasts with other studies, which show that when an mRNA delivery system is co-formulated with a TLR agonist, the expression of the delivered mRNA reduces by several orders of magnitude due to the downstream expression of pro-inflammatory cytokines inhibiting the cell's ribosomal protein synthesis machinery.[43] This effect seems to be TLR-dependent, with TLR3 activation exhibiting the most potent reduction in RNA expression, while TLR7 and TLR9 have a moderate effect and minimal effect, respectively. Once stimulated, most TLR pathways lead to the same pro-inflammatory pathways. This TLR-dependent mechanism may instead be due to the non-selective activation of other PRRs by specific adjuvants, such as polyI:C, which not only antagonises TLR3 but also cytosolic RNA sensors. In our case, the minimal effect on transfection efficiency when spiked with free Loxoribine, especially in DC2.4s, which are known to express TLR7, was an encouraging indication that adjuvancy with Loxoribine should not compromise protein expression.[31]

TLR7 activation assay. Having observed high transfection efficiencies from the Loxoribine-conjugated PBAEs in both HEK293T and DC2.4 cell lines, we then evaluated the Loxoribine-conjugated PBAEs and LOX-(pBDD-5AP)-LOX and its counterpart polyplexes to stimulate intracellular TLR7 compared with free Loxoribine. This was achieved using an engineered HEK cell line, HEK-Blue™ TLR7, transduced to co-express TLR7 with an NF-kB-inducible secreted embryonic alkaline phosphatase (SEAP) reporter gene, which can be detected by the conversion of the SEAP-induced hydrolysis of its corresponding substrate into a UV (650 nm) absorbing product (Fig. 5A). Similar to the formulation characterisation studies described earlier, polyplexes were prepared at PBAE/saRNA w/w ratios of 32, 64, and 128 using firefly luciferase encoding saRNA. Using the data from our quantification assays to determine Loxoribine conjugation, we compared the polyplexes produced to the equivalent concentrations of non-formulated LOX-(pBDD-5AP)-LOX to examine the potential synergy when complexed with saRNA, which itself can stimulate TLR7, and against free Loxoribine to determine the effect of conjugation (Fig. S4D). All formulations were assessed against Lipofectamine (serving as the positive expression control) and Triton X-100 (serving as the positive toxicity control). High metabolic activity values (>90%) were demonstrated for all treatments with no major decrease in viability for all free Loxoribine, LOX-(pBDD-5AP)-LOX and saRNA polyplex concentrations in accordance with the non-transgenic HEK293T cells tested above and therefore would not impact the expression of SEAP to assess TLR7 activation (Fig. S4A, S4C and 5C).

Because Loxoribine is covalently conjugated to the polymer backbone, its effective intracellular dose is governed by nanoparticle uptake and endosomal trafficking rather than extracellular concentration. Thus, classical dose–response analyses used for free small-molecule agonists are not directly translatable to this system. Instead, we compared free and conjugated Loxoribine at matched LOX-equivalent concentrations to assess functional preservation and enhancement of TLR7 signalling.

Quantification with the SEAP reporter revealed a dose-dependent increase in $OD_{650\ nm}$ with increasing free Loxoribine concentrations (Fig. S4B). Both free H_2N-(pBDD-5AP)-NH_2 and the resulting polyplex exhibited a lower or statistically insignificant difference in OD_{650} compared to the equivalent concentrations of free Loxoribine due to the absence of Loxoribine or weak activation of TLR7 alone by saRNA when encapsulated. Free LOX-(pBDD-5AP)-LOX exhibited a dose-dependent increase in TLR7 activation, with free polymer concentrations at the equivalent of polyplex at w/w 128 exhibiting 50% higher $OD_{650\ nm}$ than the corresponding concentration of free Loxoribine (25 μg mL^{-1}). This indicates that conjugation of LOX to the polymer enhances its TLR7 antagonisation effect (Fig. 5B). This may be due to the enhanced uptake of Loxoribine or enhanced trafficking to the endosome, where the receptor resides due to an increase in apparent size when conjugated. In addition, the LOX-(pBDD-5AP)-LOX polyplexes at w/w 128 exhibited the highest $OD_{650\ nm}$ of 0.55; this was over 2-fold higher than the equivalent concentration of free Loxoribine and was likely caused by the combination of saRNA and Loxoribine. From these results, it is reasonable to suggest that TLR7 activation of conventional mRNA polyplexes can be boosted by the addition of a TLR7 agonist, which also exhibits an increase in activity

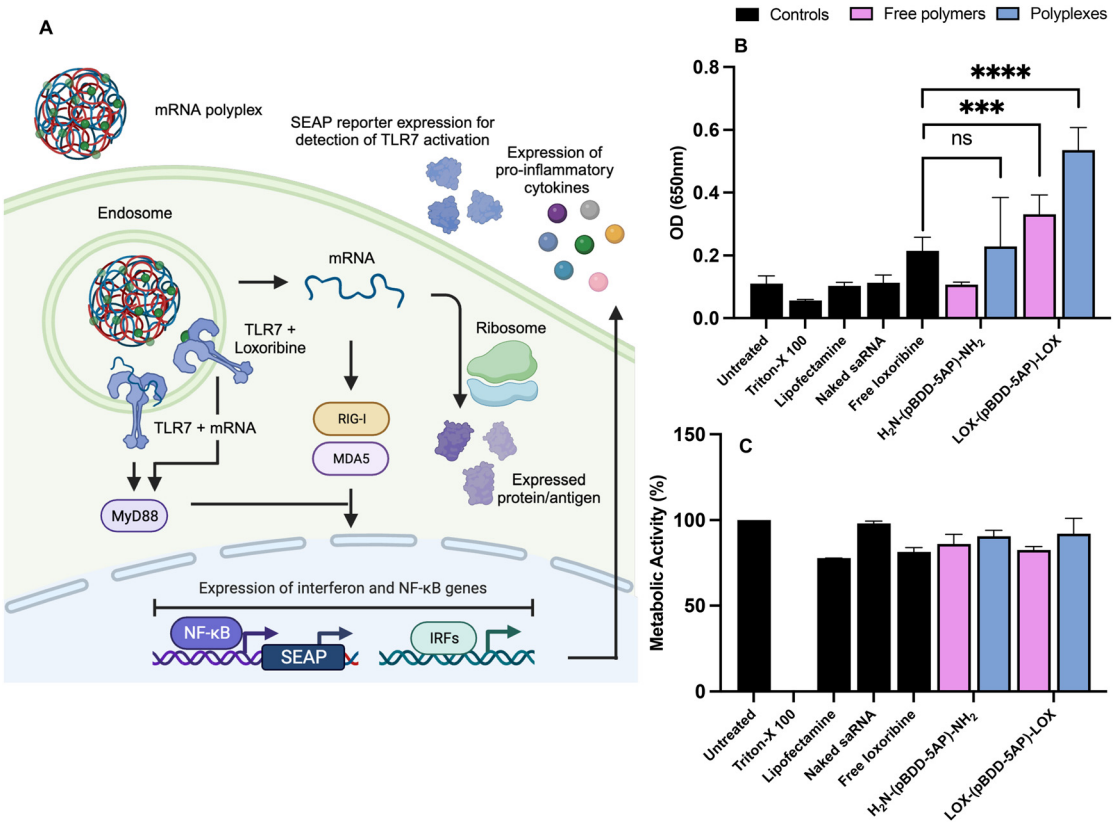

Fig. 5 TLR7 activation assay using HEK-BLUE cells. (A) Schematic of nanoparticle uptake and TLR7 activation. (B) Determination of the TLR7 activation capacity of amine and Loxoribine-end-capped polymers and nanoparticles (w/w 128) compared to controls in HEK-BLUE cells. The concentration of free lox was 25 μg mL^{-1}. (C) Metabolic activity of the amine and Loxoribine-end-capped polymers and nanoparticles (w/w 128) compared to the controls in HEK-BLUE cells. All data are presented as mean ± SD, with $n = 3$ for all conditions. Statistical significance was determined using a two-way ANOVA test, with $P < 0.05$ considered significant ($p^{***} < 0.001$ and $p^{****} < 0.0001$).

from being transported to the endosome in either nanoparticle or polymer forms. Interestingly, lipofectamine-delivered saRNA did not exhibit any statistically significant TLR7 activation over the untreated control, which may suggest a difference between the lipid and polymer delivery systems (Fig. 5B).

Cellular uptake of polyplexes. Due to the encouraging transfection, toxicity and TLR7 receptor activation profiles of the LOX-(pBDD-5AP)-LOX polyplex at w/w 128, we further investigated the extent of internalisation of these polyplexes. Therefore, we first generated a FITC-labelled LOX-(pBDD-5AP)-LOX through an isothiocyanate reaction at the pendant hydroxyl groups of the 5-AP monomers within the core PBAE. Imaging flow cytometry was utilised to evaluate the cellular uptake of the selected polyplexes at 2 h and 4 h after treatment (Fig. 6A–C). The successful cell association of the nanoparticles using DC2.4 cells was evaluated through FITC intensity, and the histogram of the 2 h and 4 h indicated the increased intensity of FITC fluorescence observed (Fig. 6B). The median fluorescence intensity value at 2 h incubation was around 60 000, and expectedly, the intensity further increased to around 80 000 at 4 h incubation. High internalisation can explain the high transfection efficiencies of the LOX-(pBDD-5AP)-LOX w/w 128 polyplexes. In addition to cellular uptake scores, the internalisation *vs.* membrane association of nanoparticles for each cell can be analysed using imaging flow cytometry. In this study, the median internalisation score of the polyplexes was approximately 1.7, indicating that a high proportion of nanoparticles were internalised inside the cells, since having a score less than 0.3 can be considered surface bound (Fig. S3).[44]

In order to assess further the intracellular internalisation mechanism of the selected nanoparticle LOX-(pBDD-5AP)-LOX w/w 128 in HEK293T and DC2.4 cells, we employed confocal microscopy to evaluate colocalization with a lysosomal (Lysotracker™ red) and nuclear (Hoechst 33342) stain (Fig. 6D). After 2 h post administration, confocal micrographs showed that polyplexes successfully internalised within the cells and merged images demonstrated minimal co-localisation with the acidic lysosomes. This was analysed using ImageJ, indicating Pearson's correlation coefficient between FITC labelled polyplexes and Lysotracker™ stained lysosomes was below 0.5 (0.3 for HEK293T and 0.4 for DC2.4 cells). Slightly higher co-localisation values were detected for DC2.4 (0.4) cells compared to HEK293T cells (0.3), which may be one of the reasons for the low transfection of dendritic cells. Given the ~200 nm particle diameters, it is likely that these formu-

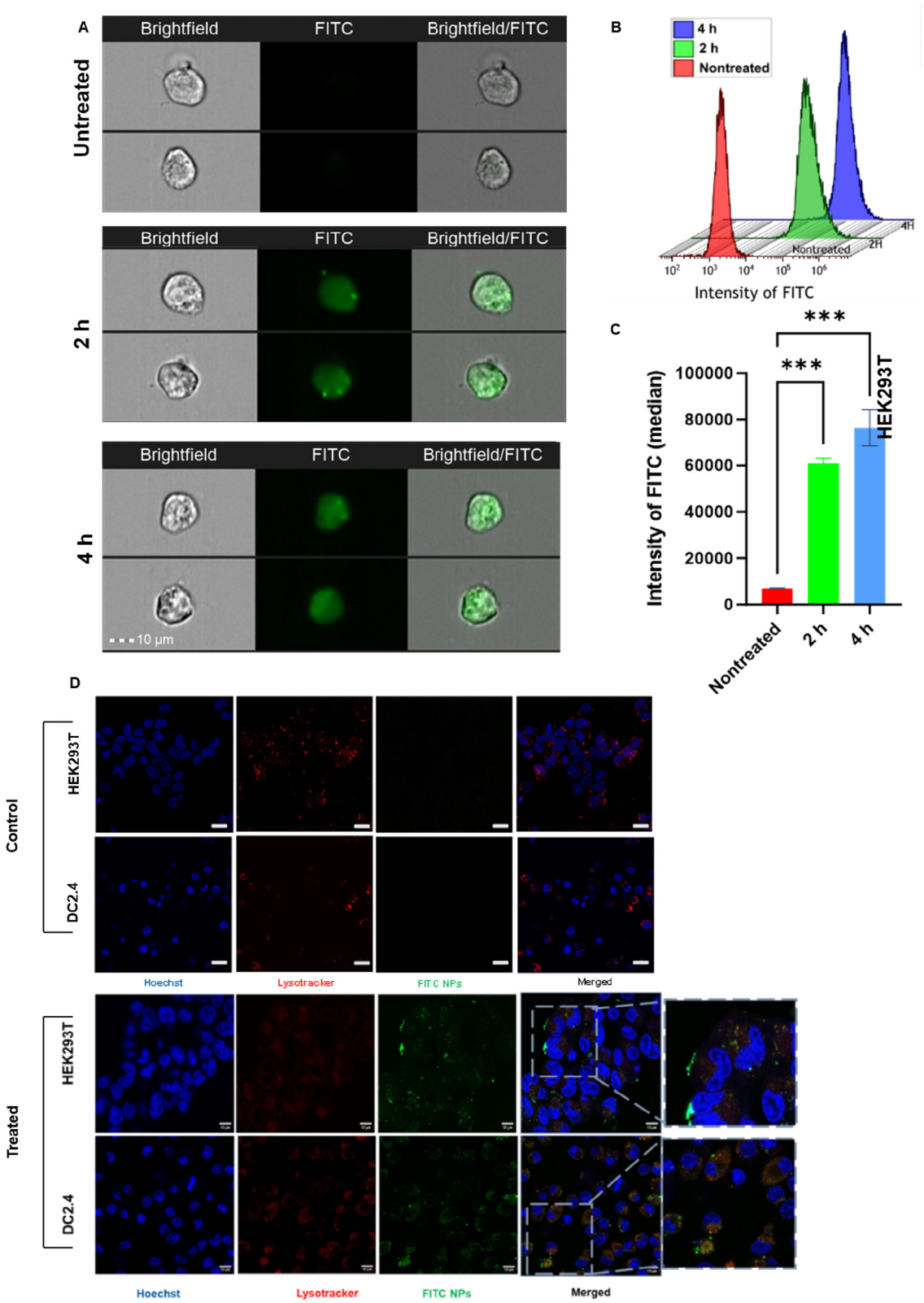

Fig. 6 Cellular uptake of PBAE-derived saRNA polyplexes. (A) Imaging flow cytometry images for DC2.4 cells after 2 h and 4 h of treatment with FITC-labelled LOX-(pBDD-5AP)-LOX polyplexes at a PBAE/saRNA w/w ratio of 128 at 500 ng per well (500 ng mL^{-1}). Scale bar: 10 μm. (B) Histograms of fluorescence intensity and (C) median fluorescence values. The data were analysed using IDEAS software and Kaluza. (D) Representative live-cell confocal microscopy images of HEK293T and DC2.4 cells for both control (untreated) and treated groups 2 h post-transfection with firefly luciferase-encoding saRNA formulated with LOX-(pBDD-5AP)-LOX at a PBAE/saRNA w/w ratio of 128 at 100 ng per well (500 ng mL^{-1}) saRNA. Scale bar: 10 μm (63x). Representative control (untreated) live-cell confocal microscopy images of HEK293T and DC2.4 cells are shown in Fig. S4.

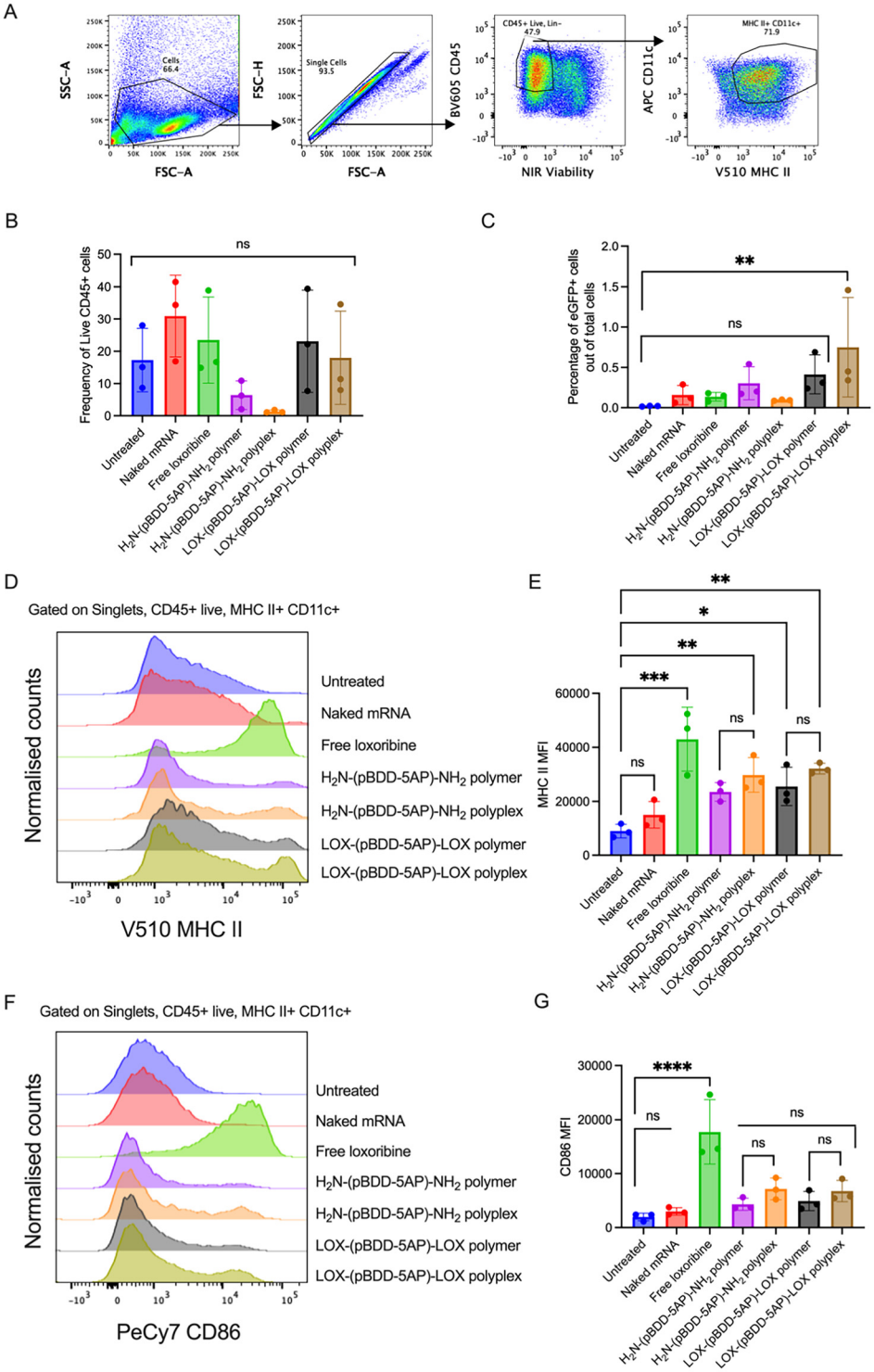

Fig. 7 BMDC transfection efficiency and activation markers after treatment with H_2N-(pBDD-5AP)-NH_2 or LOX-(pBDD-5AP)-LOX free polymers and their polyplex formulations at 1 μg mL^{-1} mRNA at an mRNA/polymer w/w ratio of 128. (A) Representative gating strategy of BM DCs. Cells were gated on singlets, live CD45+, Lin- (Linage includes CD19, B220, CD3, Ly6c, Ly6G and CD64 to gate out monocytes, neutrophils, macrophages, plasmacytoid DCs, CD4 T cells and CD8 T cells) MHC II+ CD11c+ cells. (B) Bar graph showing the frequency of live CD45+ of live singlets under different conditions. (C) Bar graph showing the percentage of eGFP+ cells out of the total live CD45+ cells. (D) Representative histogram of MHC II expression of BM DCs gated, as shown in (A). (E) Bar graph showing the MHC II mean fluorescence intensity (MFI) of each condition. (F) Representative histogram of CD86 expression of BM DCs gated, as shown in (A). (G) Bar graph showing the CD86 (MFI) of each condition. All data are presented as mean ± SD, with n = 3 for all conditions. Statistical significance was determined using a one-way ANOVA test, with $P < 0.05$ considered significant.

lations were internalised by an endocytosis mechanism. However, the apparent low colocalization with the acidic lysosomes may indicate that the particles escaped before endosomal maturation into the lysosomal compartments. This successful endosomal escape could also be due to TLR7 activation, as this is where the TLR7 receptor is and where it is activated with LOX-conjugated carriers. Although further endosomal escape studies are required to investigate this phenomenon in more detail, it is possible that enhanced endosomal escape was a factor in the high expression efficiencies observed for these complexes.

Transfection and activation of bone marrow-derived dendritic cells. To further investigate the ability of our Loxoribine-conjugated PBAEs and derived polyplexes to activate conventional Dendritic Cells (cDCs), we determined transfection and activation of primary murine bone marrow-derived cDCs (BMDCs). Given the wide body of evidence, indicating that m1ψ containing mRNA reduces the intrinsic stimulation of TLRs and other PRRs,[45,46] for these experiments, we opted to formulate polyplexes using eGFP encoding mRNA instead of saRNA. Polyplexes derived from LOX-(pBDD-5AP)-LOX and H_2N-(pBDD-5AP)-NH_2 were formulated at a polymer/mRNA w/w ratio of 128, which exhibited the highest expression in DC2.4s (Fig. 4D). The resulting polyplexes were then incubated with BMDCs at 1 μg mL^{-1} mRNA for 24 h and compared with LOX-(pBDD-5AP)-LOX and H_2N-(pBDD-5AP)-NH_2 as free polymers, free Loxoribine as a positive control and fresh media as an untreated control. Cells were analysed by flow cytometry for the expression of eGFP as a marker for transfection efficiency and CD86 and MHC II indicators of DC activation (Fig. 7A).

We observed no statistically significant changes in cell viability across the formulations. However, there was relatively large variability across the three replicates due to each replicate culture derived from individual mice (Fig. 7B). Only the LOX-(pBDD-5AP)-LOX polyplex condition displayed statistically significant eGFP expression over the untreated control, exhibiting modest 1% eGFP+ cells of the total cells collected (Fig. 7C). Free Loxoribine, the positive control, increased MHCII expression in the majority of the BM DCs. We observed an increase in MHCII expression with the polyplexes compared to the untreated control. However, there was no clear difference in MHC II expression between the control polymers (without Loxoribine conjugation) compared to the Loxoribine-conjugated PBAEs, suggesting that the polymers themselves may be intrinsically activating these pathways (Fig. 7D and E). There was a small increase in cells producing high levels of MHC II under the LOX-(pBDD-5AP)-LOX polyplex condition, indicating strong activation (Fig. 7D).

A similar expression pattern is observed for CD86, with free Loxoribine inducing high levels of CD86 with the polyplexes. There was no significant difference in MHC II between the polyplexes and polymers (Fig. 7F and G). In contrast to the findings observed from the HEK-BLUE TLR7 assay (Fig. 5), which showed that our Loxoribine-conjugated polyplex exhibited higher stimulation of the TLR7 receptor, the Loxoribine-conjugated PBAEs and derived polyplexes did not exhibit higher CD86 expression or MHCII than free Loxoribine in the BMDC model (Fig. 7D–G). This may be due to the difference in the uptake of the polymers in the BMDCs relative to the HEK-Blue cells.

Conclusion

In conclusion, the development of messenger RNA technology has accelerated the translation of innovative vaccines and treatments. The search for safe and effective delivery systems for RNA medicines has led to a focus on nanoparticle-based carriers, particularly the promising avenue of polycations, such as PBAEs. Despite challenges related to immune activation and translation efficiency, recent advances have been made towards improving these delivery systems. This study introduces a new and potentially important advance: TLR7a-conjugated polycation using Loxoribine for self-amplifying mRNA formulations. Through the synthetic pathway and formulation process, these polymers successfully encapsulated the cargo, resulting in small polyplex nanoparticles with notable transfection efficiency and minimal cytotoxicity. Importantly, the TLR7 activation assays demonstrated the significant potential of LOX-end-capped formulations to induce TLR7 signalling, surpassing amine-end-capped PBAE-based formulations and Lipofectamine. These findings highlight that the promise of LOX-end-capped formulations at a w/w ratio of 128 enhances mRNA delivery and activates crucial immune pathways. Conjugating Loxoribine directly to the polymer, rather than formulating it into an LNP, avoids the uncertainty around its positioning and retention, which is typically challenging with conventional cationic lipid-based systems. Although this work employed photo-initiated thiol–ene chemistry due to its simplicity and accessibility, we acknowledge that alternative bioorthogonal chemistries, such as tetrazine-thiol exchange with subsequent alkene locking, may offer advantages in terms of selectivity and characterisation. Incorporating these strategies represents a valuable direction for the future optimization of these delivery systems.

Author contributions

Conceptualization, H. B., C. A. and P. G.; data curation and formal analysis, H. B., A. E., R. J. K., C. G., N. G., C. L. B., C. A. and P. G.; writing – original draft preparation, H. B.; writing review and editing, H. B., A. E., R. J. K., C. G., N. G., C. L. B., C. A. and P. G.; supervision, C. A. and P. G.; project administration, C. A.; funding acquisition, H. B. and C. A. All authors have read and agreed to the published version of the manuscript.

Conflicts of interest

All authors declare that they have no conflicts of interest.

Data availability

All relevant data can be obtained from the corresponding authors upon request at p.gurnani@ucl.ac.uk and cameron.alexander@nottingham.ac.uk.

Supplementary information (SI) is available. See DOI: https://doi.org/10.1039/d5bm01812a.

Acknowledgements

We thank the Royal Society for the Wolfson Research Merit Award (WM150086 to CA). This work was supported by Wellcome Leap as part of the R3 Program [Biofoundry-in-a-Box] and by the Turkish Ministry of National Education. CG and CB were supported by PhD studentship from the Percy Stevens Foundation. We also thank Esme Ireson and Paul Cooling for expert technical support. The Nanoscale & Macroscale Research Centre (NMRC) is acknowledged for providing the facilities for TEM and related analysis particularly to Denise McLean. We thank the School of Life Sciences Imaging Facility (SLIM) and its staff, particularly Dr Tim Self, for access to facilities and expert guidance.

References

1 M. Chehelgerdi and M. Chehelgerdi, The use of RNA-based treatments in the field of cancer immunotherapy, *Mol. Cancer*, 2023, **22**(1), 106.
2 L. Miao, Y. Zhang and L. Huang, mRNA vaccine for cancer immunotherapy, *Mol. Cancer*, 2021, **20**(1), 1–23.
3 N. Pardi, M. J. Hogan, F. W. Porter and D. Weissman, mRNA vaccines—a new era in vaccinology, *Nat. Rev. Drug Discovery*, 2018, **17**(4), 261–279.
4 M. Karam and G. Daoud, mRNA vaccines: Past, present, future, *Asian J. Pharm. Sci.*, 2022, **17**(4), 491–522.
5 Z. A. Azrak, M. S. Taha, J. Jagal, A. Elsherbeny, H. Bayraktutan, M. H. AbouGhaly, A. H. Elshafeey, K. Greish and M. Haider, Optimized mucoadhesive niosomal carriers for intranasal delivery of carvedilol: A quality by design approach, *Int. J. Pharm.*, 2024, 123935.
6 N. K. Dastgerdi, N. K. Dastgerdi, H. Bayraktutan, G. Costabile, F. Atyabi, R. Dinarvand, G. Longobardi, C. Alexander and C. Conte, Enhancing siRNA cancer therapy: Multifaceted strategies with lipid and polymer-based carrier systems, *Int. J. Pharm.*, 2024, 124545.
7 A. Akinc, M. A. Maier, M. Manoharan, K. Fitzgerald, M. Jayaraman, S. Barros, S. Ansell, X. Du, M. J. Hope and T. D. Madden, The Onpattro story and the clinical translation of nanomedicines containing nucleic acid-based drugs, *Nat. Nanotechnol.*, 2019, **14**(12), 1084–1087.
8 P. Gurnani, A. K. Blakney, J. Yeow, C. R. Bouton, R. J. Shattock, M. M. Stevens and C. Alexander, An improved synthesis of poly (amidoamine) s for complexation with self-amplifying RNA and effective transfection, *Polym. Chem.*, 2020, **11**(36), 5861–5869.
9 B. Fayed, J. Jagal, R. Cagliani, R. A. Kedia, A. Elsherbeny, H. Bayraktutan, G. Khoder and M. Haider, Co-administration of amoxicillin-loaded chitosan nanoparticles and inulin: A novel strategy for mitigating antibiotic resistance and preserving microbiota balance in Helicobacter pylori treatment, *Int. J. Biol. Macromol.*, 2023, **253**, 126706.
10 H. Bayraktutan, P. Symonds, V. A. Brentville, C. Moloney, C. Galley, C. L. Bennett, A. Mata, L. Durrant, C. Alexander and P. Gurnani, Sparsely PEGylated poly (beta-amino ester) polyplexes enhance antigen specific T-cell response of a bivalent SARS-CoV-2 DNA vaccine, *Biomaterials*, 2024, 122647.
11 P. Gurnani, A. K. Blakney, R. Terracciano, J. E. Petch, A. J. Blok, C. R. Bouton, P. F. McKay, R. J. Shattock and C. Alexander, The *in vitro*, *ex vivo*, and *in vivo* effect of polymer hydrophobicity on charge-reversible vectors for self-amplifying RNA, *Biomacromolecules*, 2020, **21**(8), 3242–3253.
12 C. Fornaguera, J. F. Alarcon, A. Masoero, I. Pagnotta, R. Vaya, P. Castells-Colldeforns, M. Losada, M. Guarro, M. Lecina and G. Sitia, Polymeric nanoparticle-loaded extracellular vesicles as biomimetic nucleic acid vaccines, *Research Square*, 2025, DOI: 10.21203/rs.3.rs-7030394/v1.
13 K. M. Steinegger, L. Allmendinger, S. Sturm, F. Sieber-Schäfer, A. P. Kromer, K. Müller-Caspary, B. Winkeljann and O. M. Merkel, Molecular dynamics simulations elucidate the molecular organization of poly (beta-amino ester) based polyplexes for siRNA delivery, *Nano Lett.*, 2024, **24**(49), 15683–15692.
14 H. Bayraktutan, R. Kopiasz, A. Elsherbeny, P. Gurnani and C. Alexander, Poly (beta-amino esters): applications in immunology, *Chem. Sci.*, 2026, **17**, 850–879.
15 N. Puigmal, V. Ramos, N. Artzi and S. Borrós, Poly (β-amino ester) s-based delivery systems for targeted transdermal vaccination, *Pharmaceutics*, 2023, **15**(4), 1262.
16 M. Navalón-López, A. Dols-Perez, S. Grijalvo, C. Fornaguera and S. Borrós, Unravelling the role of individual components in pBAE/polynucleotide polyplexes in the synthesis of tailored carriers for specific applications: on the road to rational formulations, *Nanoscale Adv.*, 2023, **5**(6), 1611–1623.
17 N. Qiao, M. Hori, M. Naito, H. Chang, S. Ogura, M. Suzuki, T. Kimura, S. Fukushima, H. J. Kim and S. Uchida, Increasing polycation hydrophobicity in mRNA polyplex vaccines enhances the efficacy of humoral and cellular immunity induction, *Biomaterials*, 2026, **324**, 123515.
18 P. Dosta, A. M. Cryer, M. Z. Dion, T. Shiraishi, S. P. Langston, D. Lok, J. Wang, S. Harrison, T. Hatten and M. L. Ganno, Investigation of the enhanced antitumour potency of STING agonist after conjugation to polymer nanoparticles, *Nat. Nanotechnol.*, 2023, **18**(11), 1351–1363.
19 U. Sahin, K. Karikó and Ö Türeci, mRNA-based therapeutics—developing a new class of drugs, *Nat. Rev. Drug Discovery*, 2014, **13**(10), 759–780.
20 F. Heil, P. Ahmad-Nejad, H. Hemmi, H. Hochrein, F. Ampenberger, T. Gellert, H. Dietrich, G. Lipford, K. Takeda and S. Akira, The Toll–like receptor 7 (TLR7)–specific stimulus loxoribine uncovers a strong relationship within the TLR7, 8 and 9 subfamily, *Eur. J. Immunol.*, 2003, **33**(11), 2987–2997.

21 V. Gote, P. K. Bolla, N. Kommineni, A. Butreddy, P. K. Nukala, S. S. Palakurthi and W. Khan, A comprehensive Review of mRNA vaccines, *Int. J. Mol. Sci.*, 2023, **24**(3), 2700.
22 S. Qin, X. Tang, Y. Chen, K. Chen, N. Fan, W. Xiao, Q. Zheng, G. Li, Y. Teng and M. Wu, mRNA-based therapeutics: powerful and versatile tools to combat diseases, *Signal Transduct. Target. Ther.*, 2022, **7**(1), 166.
23 A. Elsherbeny, H. Bayraktutan, U. C. Oz, C. Moloney, J. C. Ashworth, A. M. Grabowska and C. Alexander, Responsive Nanomaterial Delivery Systems for Pancreatic Cancer Management, *Adv. Ther.*, 2023, 2300330.
24 A. Kowalczyk, F. Doener, K. Zanzinger, J. Noth, P. Baumhof, M. Fotin-Mleczek and R. Heidenreich, Self-adjuvanted mRNA vaccines induce local innate immune responses that lead to a potent and boostable adaptive immunity, *Vaccine*, 2016, **34**(33), 3882–3893.
25 A. A. Smith, E. C. Gale, G. A. Roth, C. L. Maikawa, S. Correa, A. C. Yu and E. A. Appel, Nanoparticles Presenting Potent TLR7/8 Agonists Enhance Anti-PD-L1 Immunotherapy in Cancer Treatment, *Biomacromolecules*, 2020, **21**(9), 3704–3712.
26 M. Luchner, S. Reinke and A. Milicic, TLR agonists as vaccine adjuvants targeting cancer and infectious diseases, *Pharmaceutics*, 2021, **13**(2), 142.
27 D. N. Toussi and P. Massari, Immune adjuvant effect of molecularly-defined toll-like receptor ligands, *Vaccines*, 2014, **2**(2), 323–353.
28 N. Chaudhary, L. N. Kasiewicz, A. N. Newby, M. L. Arral, S. S. Yerneni, J. R. Melamed, S. T. LoPresti, K. C. Fein, D. M. Strelkova Petersen and S. Kumar, Amine headgroups in ionizable lipids drive immune responses to lipid nanoparticles by binding to the receptors TLR4 and CD1d, *Nat. Biomed. Eng.*, 2024, **8**(11), 1483–1498.
29 A. E. Zelkoski, Z. Lu, G. Sukumar, C. Dalgard, H. Said, M.-G. Alameh, E. Mitre and A. M. Malloy, Ionizable lipid nanoparticles of mRNA vaccines elicit NF-κB and IRF responses through toll-like receptor 4, *npj Vaccines*, 2025, **10**(1), 73.
30 S. Abbasi and S. Uchida, Multifunctional immunoadjuvants for use in minimalist nucleic acid vaccines, *Pharmaceutics*, 2021, **13**(5), 644.
31 A. K. Blakney, P. F. McKay, C. R. Bouton, K. Hu, K. Samnuan and R. J. Shattock, Innate inhibiting proteins enhance expression and immunogenicity of self-amplifying RNA, *Mol. Ther.*, 2021, **29**(3), 1174–1185.
32 B. Wilson and K. M. Geetha, Lipid nanoparticles in the development of mRNA vaccines for COVID-19, *J. Drug Deliv. Sci. Technol.*, 2022, **74**, 103553.
33 A. M. Weiss, S. Hossainy, S. J. Rowan, J. A. Hubbell and A. P. Esser-Kahn, Immunostimulatory polymers as adjuvants, immunotherapies, and delivery systems, *Macromolecules*, 2022, **55**(16), 6913–6937.
34 J. Huete-Carrasco, R. I. Lynch, R. W. Ward and E. C. Lavelle, Rational design of polymer–based particulate vaccine adjuvants, *Eur. J. Immunol.*, 2023, 2350512.
35 H. Bayraktutan, R. J. Kopiasz, A. Elsherbeny, M. M. Espuga, N. Gumus, U. C. Oz, K. Polra, P. F. McKay, R. J. Shattock and P. Ordóñez-Morán, Polysarcosine functionalised cationic polyesters efficiently deliver self-amplifying mRNA, *Polym. Chem.*, 2024, **15**(18), 1862–1876.
36 N. K. Dastgerdi, N. Gumus, H. Bayraktutan, D. Jackson, K. Polra, P. F. McKay, F. Atyabi, R. Dinarvand, R. J. Shattock and L. Martinez-Pomares, Charge neutralized poly (β-amino ester) polyplex nanoparticles for delivery of self-amplifying RNA, *Nanoscale Adv.*, 2024, **6**, 1409–1422.
37 G. T. Zugates, N. C. Tedford, A. Zumbuehl, S. Jhunjhunwala, C. S. Kang, L. G. Griffith, D. A. Lauffenburger, R. Langer and D. G. Anderson, Gene delivery properties of end-modified poly (β-amino ester) s, *Bioconjugate Chem.*, 2007, **18**(6), 1887–1896.
38 N. M. Hamelmann, S. Uijttewaal, S. D. Hujaya and J. M. Paulusse, Enhancing Cellular Internalization of Single-Chain Polymer Nanoparticles via Polyplex Formation, *Biomacromolecules*, 2022, **23**(12), 5036–5042.
39 S. K. Filippov, R. Khusnutdinov, A. Murmiliuk, W. Inam, L. Y. Zakharova, H. Zhang and V. V. Khutoryanskiy, Dynamic light scattering and transmission electron microscopy in drug delivery: a roadmap for correct characterization of nanoparticles and interpretation of results, *Mater. Horiz.*, 2023, **10**(12), 5354–5370.
40 C. H. Jones, M. Chen, A. Ravikrishnan, R. Reddinger, G. Zhang, A. P. Hakansson and B. A. Pfeifer, Mannosylated poly (beta-amino esters) for targeted antigen presenting cell immune modulation, *Biomaterials*, 2015, **37**, 333–344.
41 Z. Zhang, K. Wen, C. Zhang, F. Laroche, Z. Wang, Q. Zhou, Z. Liu, J. P. Abrahams and X. Zhou, Extracellular nanovesicle enhanced gene transfection using polyethyleneimine in HEK293T cells and zebrafish embryos, *Front. Bioeng. Biotechnol.*, 2020, **8**, 448.
42 I. González-Domínguez, E. Puente-Massaguer, J. Lavado-García, L. Cervera and F. Gòdia, Micrometric DNA/PEI polyplexes correlate with higher transient gene expression yields in HEK 293 cells, *New Biotechnol.*, 2022, **68**, 87–96.
43 E. Ben-Akiva, J. Karlsson, S. Hemmati, H. Yu, S. Y. Tzeng, D. M. Pardoll and J. J. Green, Biodegradable lipophilic polymeric mRNA nanoparticles for ligand-free targeting of splenic dendritic cells for cancer vaccination, *Proc. Natl. Acad. Sci. U. S. A.*, 2023, **120**(26), e2301606120.
44 Y. Phanse, A. E. Ramer-Tait, S. L. Friend, B. Carrillo-Conde, P. Lueth, C. J. Oster, G. J. Phillips, B. Narasimhan, M. J. Wannemuehler and B. H. Bellaire, Analyzing cellular internalization of nanoparticles and bacteria by multi-spectral imaging flow cytometry, *J. Visualized Exp.*, 2012, **64**, e3884.
45 T. E. Mulroney, T. Pöyry, J. C. Yam-Puc, M. Rust, R. F. Harvey, L. Kalmar, E. Horner, L. Booth, A. P. Ferreira and M. Stoneley, N 1-methylpseudouridylation of mRNA causes + 1 ribosomal frameshifting, *Nature*, 2024, **625**(7993), 189–194.
46 K. Karikó, H. Muramatsu, F. A. Welsh, J. Ludwig, H. Kato, S. Akira and D. Weissman, Incorporation of pseudouridine into mRNA yields superior nonimmunogenic vector with increased translational capacity and biological stability, *Mol. Ther.*, 2008, **16**(11), 1833–1840.